Interplay of conventional with inverse electrocaloric response in $(Pb,Nb)(Zr,Sn,Ti)O_3$ antiferroelectric materials

Nikola Novak,[1,2,*] Florian Weyland,[1] Satyanarayan Patel,[1] Hanzheng Guo,[3] Xiaoli Tan,[3] Jürgen Rödel,[1] and Jurij Koruza[1]

[1]*Institute of Materials Science, Technische Universität Darmstadt, Alarich-Weiss-Straße 2, 64287 Darmstadt, Germany*
[2]*Jožef Stefan Institute, Jamova 39, 1000 Ljubljana, Slovenia*
[3]*Department of Materials Science and Engineering, Iowa State University, Ames, Iowa 50011, USA*

The electrocaloric effect in ferroics is considered a powerful solid-state cooling technology. Its potential is enhanced by correlation to the inverse electrocaloric effect and leads into mechanisms of decreasing or increasing dipolar entropy under applied electric field. Nevertheless, the mechanism underlying the increase of the dipolar entropy with applied electric field remains unclear and controversial. This study investigates the electrocaloric response of the antiferroelectric $Pb_{0.99}Nb_{0.02}[(Zr_{0.58}Sn_{0.43})_{0.92} Ti_{0.08}]_{0.98}O_3$ in which the critical electric field is low enough to induce the ferroelectric phase over a broad temperature range. Utilizing temperature- and electric-field-dependent dielectric measurements, direct electrocaloric measurements, and *in situ* transmission electron microscopy, a crossover from conventional to inverse electrocaloric response is demonstrated. The origin of the inverse electrocaloric effect is rationalized by investigating the field-induced phase transition between antiferroelectric and ferroelectric phases. The disappearance of the latent heat at field-induced transition coincides with the crossover of the electrocaloric effect and demonstrates that the overall electrocaloric response is an interplay of different entropy contributions. This opens new opportunities for highly efficient, environmentally friendly cooling devices based on ferroic materials.

Nearly 20% of the residential electricity consumption in EU is used for cooling and air-conditioning devices, representing one of the major sources of environmental pollution [1]. This was also recognized by the European Union, triggering the first regulation on certain fluorinated greenhouse gases in 2006 [2]. The new legislation reinforced the interest in solid-state refrigerators based on caloric materials, which are considered a viable alternative to the existing cooling technologies based on the mechanical vapor-compression cycle using greenhouse gases [3,4]. In caloric materials, the heating/cooling effect is caused by the change of the configurational entropy upon application/removal of external stimuli, such as magnetic, electric, or mechanical field [5–7]. Electrocaloric materials attract considerable interest due to ease of application of the electric field and reduced cost in comparison to magnetocalorics or barocalorics. For the conventional electrocaloric effect (ECE), the application of an electric field increases ordering of the polarization and thus decreases the dipolar entropy. Under adiabatic conditions of a (nearly) reversible process, this entropy decrease leads to heating. Subsequently, removal of the electric field decreases dipole ordering and causes an increase of the dipolar entropy accompanied by cooling of the material [8,9].

Recent studies on relaxor ferroelectrics (FEs) and antiferroelectrics (AFEs) revealed the presence of the inverse/negative electrocaloric effect; i.e., materials cool when the field is applied and heat when it is removed [10–13]. Such behavior is unexpected because it requires an increase in the dipolar entropy during application of an electric field and hence a decrease in ordering of the dipolar system. While a general explanation of this phenomenon is not available, initial theories were proposed for individual systems [13,14].

For the relaxor [001]-oriented $PbMg_{1/3}Nb_{2/3}O_3 - 0.30$ $PbTiO_3$ (PMN-0.30PT) single crystal the inverse ECE was observed in the vicinity of the inter-ferroelectric transition between the rhombohedral and tetragonal phases and was attributed to the electric-field-induced phase transition [9,10]. The tetragonal and rhombohedral phases do not share group-subgroup relations. This transition is therefore of first order, which is characterized by the presence of the latent heat [8,15]. In general, inverse ECE can be expected at electric-field-induced inter-ferroelectric phase transitions from lower to higher symmetry phase, if the entropy change due to the structural phase transition is higher than the dipolar entropy change.

The inverse ECE in AFEs has been reported for several systems by utilizing indirect and direct measurement methods [12–14,16]. Phenomenological calculations and indirect measurements indicate that an inverse ECE in AFEs can be observed for applied electric fields below the critical field at which the ferroelectric phase is induced [13,14]. This is supported by the results of the direct ECE measurement on undoped and Ba-doped $PbZrO_3$ (PZ) where the applied electric fields were not high enough to induce the ferroelectric phase and the inverse ECE has been reported for the whole investigated temperature range [13,16]. The absence of an electric-field-induced phase transition in undoped PZ and Ba-doped PZ suggests that the origin of the inverse ECE in this AFE is most likely due to the dipolar ordering in the antiferroelectric sublattices [14]. Furthermore, the theoretically determined electric field–temperature phase diagram reveals the presence

———

*Corresponding author: novak@ceramics.tu-darmstadt.de

of a tricritical point [13]. At the tricritical point the metastable ferroelectric, antiferroelectric, and paraelectric phases merge.

In this work we investigate the ECE response of the antiferroelectric $Pb_{0.99}Nb_{0.02}[(Zr_{0.58}Sn_{0.43})_{0.92}Ti_{0.08}]_{0.98}O_3$ (abbreviated as PNZST) ceramic in which the critical electric field is low enough to induce the FE phase over a broad temperature range. The dielectric measurement under different electric fields, thermometry, and polarization response of PNZST were analyzed to establish the isofield and isothermal electric field–temperature phase diagrams and to identify the position of the triple point. The antiferroelectric microstructure and its response to applied electric fields are examined *in situ* with transmission electron microscopy (TEM). Utilizing the direct electrocaloric method, the electrocaloric temperature change as function of temperature and electric field was determined. The temperature profile of the ECE is correlated with temperature-dependent latent heat response and antiferroelectric coupling strength.

I. METHODS

The antiferroelectric ceramics with chemical formula $Pb_{0.99}Nb_{0.02}[(Zr_{0.58}Sn_{0.43})_{0.92}Ti_{0.08}]_{0.98}O_3$ (abbreviated as PNZST) were prepared by the mixed-oxide route, as described elsewhere [17]. The sintered samples were ground to a thickness of 200 μm and annealed at 670 K for 0.5 h. Silver electrodes were sputtered on the sample's planar surfaces and two thin copper wires were attached with a silver paste, providing electrical contact. A small glass-embedded thermistor was attached to one side of the sample to trace the temperature for thermometry and direct electrocaloric measurement.

The dielectric constant was obtained during heating and cooling with a rate of 2 K min^{-1}. Polarization and thermometry measurements were conducted simultaneously. Before each measurement the sample was heated to 450 K, cooled to 240 K, and finally stabilized at the measured temperature within ± 2 mK. The electric field was slowly cycled linearly with the frequency of 1 mHz between ± 4.5 kV mm^{-1}. For the direct electrocaloric measurement, a step function of the electric field was used to enforce the adiabatic condition when the field is applied. Detailed descriptions of polarization, thermometry, and direct electrocaloric measurements are reported elsewhere [18]. For TEM experiments, disk specimens (3 mm in diameter) were machined using standard procedures including grinding, cutting, dimpling, and ion milling. The dimpled disks were annealed at 473 K for 2 h to minimize residual stresses before Ar-ion milling to the point of electron transparency. Conventional and electric field *in situ* TEM experiments were carried out using a microscope operated at 200 kV.

II. RESULTS AND DISCUSSION

A. Isofield dielectric measurements

Figure 1(a) depicts the frequency-dependent real and imaginary part of the relative dielectric permittivity obtained in the heating run. The low-temperature anomaly at 304 K marks the phase transition from low-temperature rhombohedral ferroelectric phase (FE$_R$) to the tetragonal antiferroelectric phase (AFE$_T$), while the high-temperature anomalies at 411.5 K and 453 K correspond to the phase transitions from AFE$_T$ to the
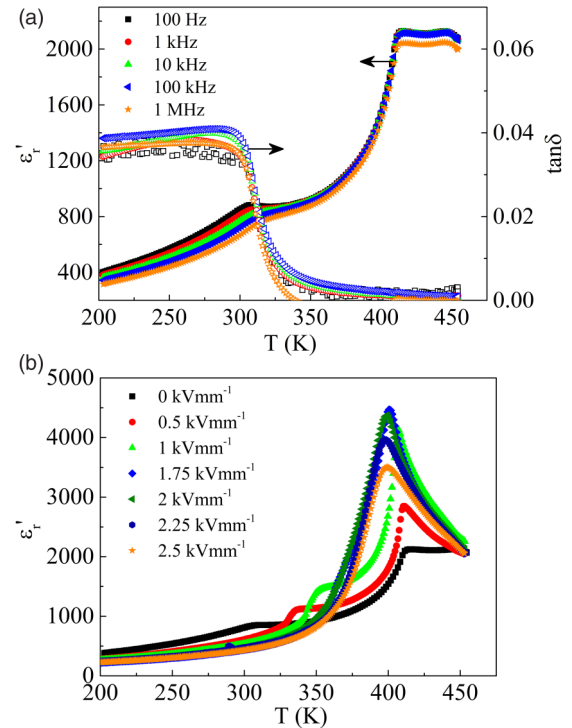
FIG. 1. (a) Real part of the relative permittivity and dielectric losses in PNZST on heating. (b) Real part of the relative permittivity obtained at different bias electric fields. The dielectric response was measured at field heating (FH) after field cooling (FC).

paraelectric multicell cubic and to the paraelectric single-cell cubic phases, respectively [19–21]. A relatively large deviation in the dielectric response between zero-field heating (ZFH) and zero-field cooling (ZFC) measurement in the temperature range between 240 K and 380 K has been observed. A significant thermal hysteresis of the low-temperature FE$_R$-AFE$_T$ phase transition ($\delta T \cong 73$ K) emphasizes the importance of the measurement procedure to avoid thermal hysteresis effects. In contrast to the FE$_R$-AFE$_T$ phase transition, the AFE$_T$-PE transition temperature features a relatively small hysteresis of $\delta T \cong 1.5$ K [22]. Figure 1(b) provides the field heating dielectric response after field cooling at different dc electric fields. With increasing the electric field the FE$_R$-AFE$_T$ transition temperature increases, while the AFE$_T$-PE transition temperature decreases.

Sharp and pronounced anomalies of dielectric loss depicted in Fig. 2(a) quantify the phase transition temperatures at different electric fields. The corresponding isofield electric field–temperature (E - T) phase diagram obtained under field-heating conditions, displayed in Fig. 2(b), quantifies the impact of electric field on phase transition temperatures. The isofield E-T phase diagram of PNZST reveals two interesting features: (i) The critical field, E_{AFE-FE}, at which the ferroelectric phase is induced, increases with increasing temperature, which is in contradiction to the behavior observed in other PZ-based antiferroelectrics [14]. (ii) The AFE$_T$-PE transition temperature shifts towards lower temperatures. The behavior of E_{AFE-FE} with temperature can be understood by considering the phase transition sequence in the antiferroelectric material. In some of the PZ-based antiferroelectrics a
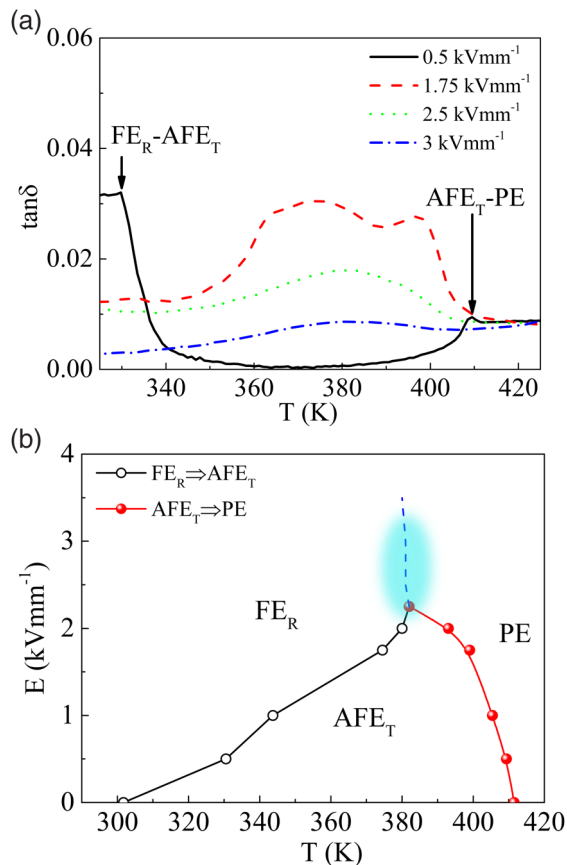
FIG. 2. (a) Dielectric losses as a function of temperature and electric field in PNZST. The anomalies indicate the phase transition temperature between the ferroelectric, antiferroelectric, and paraelectric phases. (b) Isofield E-T phase diagram reveals the presence of the triple point around 380 K and 2.25 kV mm^{-1}. The shadowed area marks the estimated electric field and temperature phase coexistence regime around the triple point.

FIG. 3. (a) Polarization hysteresis loops obtained at different temperatures underpin the shift of the $E_{\mathrm{AFE-FE}}$ towards higher electric fields with increasing temperature. (b) Thermometry measurement at different temperatures reveal a sharp increase in the sample's temperature as a consequence of released latent heat at field-induced phase transition. (c)–(e) Bright-field TEM micrographs of a [001]-oriented grain at different electric fields feature a transition from a pure AFE$_T$ phase at zero electric field into pure FE$_R$ phase at 3.3 kV mm^{-1} through a two-phase mixture (with the AFE phase of fringe contrast at the upper-left corner, and the FE phase of contrast-free appearance) at an intermediate field of 1.7 kV mm^{-1}. The inset depicts the corresponding [001] zone-axis electron diffraction patterns.

high-temperature ferroelectric phase separates the antiferroelectric and paraelectric phases [19,23]. Hence, with increasing the temperature a ferroelectric phase is approached and the energy barrier between the antiferroelectric and ferroelectric phases decreases. The reduction of the energy barrier between the two phases results in a decrease of $E_{\mathrm{AFE-FE}}$ with temperature. In PNZST the phase transition sequence is FE$_R$-AFE$_T$-PE. Therefore, the energy barrier between the antiferroelectric and ferroelectric phases increases with increasing temperature and consequently $E_{\mathrm{AFE-FE}}$ increases with temperature. The shift of the AFE$_T$-PE temperature towards lower temperatures under applied electric fields can be discussed by considering Kittel's model [24]. Antiferroelectrics can be described by two sublattices with antiparallel aligned polarization. The sublattice polarization oriented antiparallel to the field decreases upon application of electric field and eventually switches at high enough fields. The switching of the sublattice polarization may occur through the cubic phase, which could be responsible for the decrease of the AFE$_T$-PE transition temperature. However, to resolve this question polarization switching and structural investigations have to be contemplated simultaneously. At 2.25 kV mm^{-1} the FE$_R$-AFE$_T$ and AFE$_T$-PE transition tem-

peratures merge together into a triple point. The temperature-dependent dielectric permittivity and dielectric loss above 2.25 kV mm^{-1} are suppressed and broaden. A weak shoulder in dielectric loss can still be observed above 2.25 kV mm^{-1} due to the orientational heterogeneity of the polycrystalline ceramics [25–27]. The weak shoulder in dielectric loss shifts with electric field and persists up to 3.5 kV mm^{-1}. The presence of the shoulder in dielectric loss indicates the electric field and temperature convergence regime around the triple point [25].

B. Isothermal polarization, thermometry, and TEM observations

The antiferroelectric phase can be transformed into a ferroelectric phase by applying a sufficiently strong electric field $E \geqslant E_{\mathrm{AFE-FE}}$ [19–21,28]. However, not much information is available about the nature of this field-induced transition or the temperature dependency of the $E_{\mathrm{AFE-FE}}$. Therefore, a simultaneous measurement of polarization hysteresis loops and thermometry under isothermal conditions has been performed on annealed samples, depicted in Figs. 3(a) and 3(b).

A sharp polarization increase at the critical field marks the field-induced AFE_T-FE_R phase transition. The discontinuous step in polarization at E_{AFE-FE} is accompanied by a sharp increase in the sample's temperature (ΔT_S). Since the electric field was ramped slowly (1 mHz), the sharp change in temperature corresponds to the release of the latent heat and thus confirms the first-order nature of this transition [27,29]. With increasing temperature the peak of the sample's temperature decreases and shifts towards higher electric fields. A decrease in ΔT_S indicates that the first-order transition gets weaker and the amount of released latent heat is reduced [30]. The field-induced transition from AFE_T to FE_R state at room temperature could also be confirmed by *in situ* electric field TEM observation. Figures 3(c)–3(e) display the evolution of FE_R phase with increasing electric field. Figure 3(c) highlights an initially AFE_T grain transforming to a two-phase mixture [see Fig. 3(d)] at an intermediate field and to the final FE_R phase at a high field [see Fig. 3(e)].

From the hysteresis and thermometry measurements, the isothermal E-T phase diagram was constructed [see Fig. 4(a)]. The E-T phase diagram features the temperature-dependent critical electric field for FE_R and AFE_T phases. In comparison to other antiferroelectrics, where E_{AFE-FE} typically decreases with increasing temperature, the temperature dependence of E_{AFE-FE} in PNZST reveals a more complex behavior [14,31,32]. In the temperature range of the FE_R phase, the electric field of the transformation from unpoled ferroelectric phase into an ordered/poled ferroelectric phase corresponds to the coercive field. At the FE_R-AFE_T transition temperature (304 K) a sharp increase in the critical field is observed. In the AFE_T temperature range the E_{AFE-FE} increases with increasing temperature and features a peak around 380 K. The change of the sample's temperature has been traced during the increase of electric field and is depicted in Fig. 4(b). The ΔT_S decreases with increasing temperature and vanishes at 380 K. The decrease of the sample's temperature change, hence reduction of released latent heat, indicates weakening of the field-induced first-order phase transition. In the vicinity of 380 K the ΔT_S almost completely vanishes and indicates a change of the nature of field-induced transition from first to second order. It is corroborated by a change in the slope of the polarization evolution under applied electric field, which transforms from a discontinuous jump to a continuous evolution.

C. Electrocaloric response

The temperature-dependent adiabatic electrocaloric temperature change (ΔT_{EC}) for PNZST antiferroelectric ceramic is presented in Fig. 5(a) for different electric fields. Conventional ECE is observed in the temperature range between 240 K and ~380 K. The ECE is rather small between 240 K and 320 K ($\Delta T_{EC} \sim 0.2$ K), characteristic for the ferroelectric region. Despite the fact that the FE_R-AFE_T transition occurs at 304 K this small conventional ferroelectric ECE response expands well into the AFE_T temperature region (to 320 K), which is due to the electric field hysteresis of the AFE_T-FE_R phase transition. As a consequence of this hysteresis, remanent polarization (P_r) remains high above the FE_R-AFE_T phase transition temperature. At 320 K a sharp decrease in P_r correlates with an increase in ΔT_{EC}, indicating the full reversibility
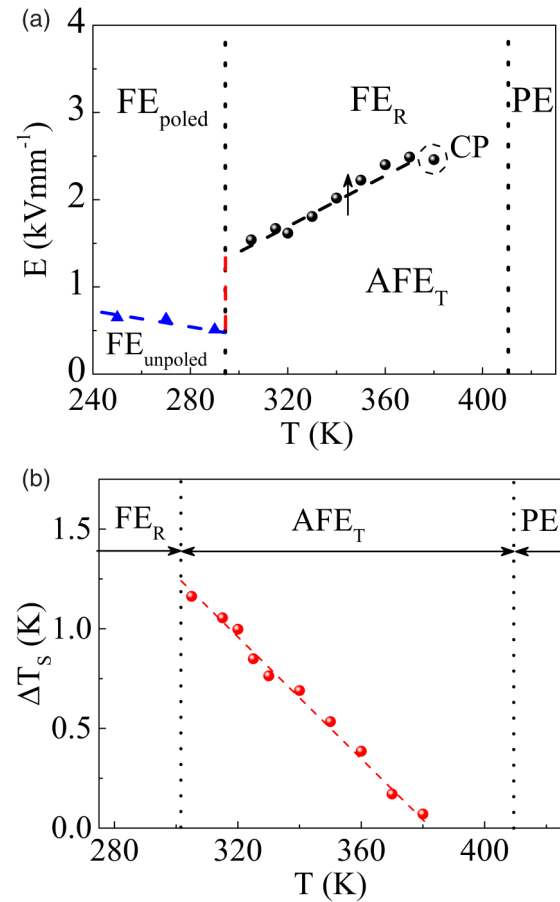
FIG. 4. (a) Stability of ferroelectric and antiferroelectric phases in PNZST ceramic is quantified in an electric field–temperature phase diagram. The arrow denotes the direction of the field-induced phase transition (isothermal experiment). Dotted lines represent the transition temperatures determined from ZFH dielectric measurements. The position of the critical point (CP) is marked by a dashed circle. (b) The change in the sample's temperature during linearly increasing/decreasing the electric field mimics the released latent heat at the field-induced AFE_T-FE_R phase transition. The change of the sample's temperature decreases with increasing temperature.

of the field-induced transition within half of the electric field cycle [22]. Hence, an additional contribution from the latent heat at the FE_R-AFE_T transition adds to ΔT_{EC}. At ~320 K the contribution from the released latent heat accounts for nearly ~50% of the overall ECE. The reduced contribution of the latent heat with increasing temperature [see Fig. 4(b)] stimulates a decrease in cooling effect. At ~380 K a crossover from conventional to inverse ECE at 2 kV mm^{-1} can be observed. The inverse ECE is present in the temperature and electric field range of ~380–410 K and 0–3 kV mm^{-1}, while above 3 kV mm^{-1} conventional ECE is demonstrated. Above ~410 K conventional ECE is obtained for all measured electric fields.

Phenomenological modeling reveals that the inverse ECE in antiferroelectrics is expected at $E < E_{AFE-FE}$ while conventional ECE is observed at $E > E_{AFE-FE}$ due to induced FE ordering [13]. Such a strict separation of the regions of inverse and conventional ECE is possible only for antiferroelectric materials with a high antiferroelectric coupling strength, which
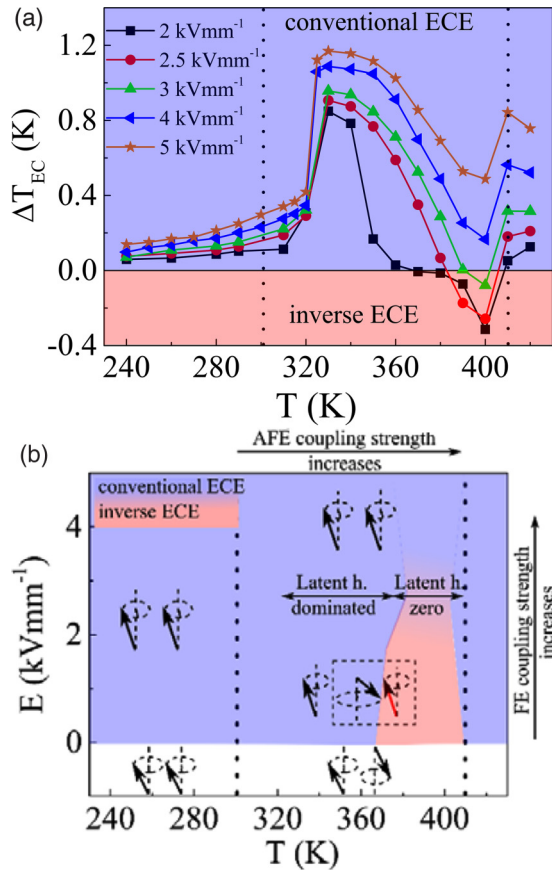
FIG. 5. (a) The ECE of PNZST ceramic features a crossover from conventional (cooling) to inverse (heating) response, considering the effect upon field removal. The ECE was measured by the direct method. The dotted lines represent the phase transition temperatures obtained from ZFH dielectric measurements. (b) Schematic representation of a possible mechanism responsible for electrocaloric behavior of PNZST. The arrows represent the alignment of polarization in temperature–electric field space. The red arrow represents the flipped polarization due to field-induced phase transition.

requires high $E_{\mathrm{AFE-FE}}$ to induce the ferroelectric phase [24,33]. High AFE coupling strength increases the critical electric field and hinders flipping of the antiparallel-oriented sublattice polarization [33]. Hence, an electric field with $E < E_{\mathrm{AFE-FE}}$ is only influencing the misalignment of the antiparallel sublattice polarization, which leads to an increase of the sublattice dipolar entropy and inverse ECE [14]. If the AFE coupling strength is weak, lower electric fields suffice to induce the ferroelectric phase and flipping of the antiparallel-oriented sublattice polarization is facilitated. As a consequence a mixture of ferroelectric and antiferroelectric phases can be present at fields $E < E_{\mathrm{AFE-FE}}$. Relatively low electric fields, required to induce the ferroelectric phase in the investigated PNZST ceramic, indicate that AFE coupling strength is much weaker in comparison to the pure PZ ceramic. This is also confirmed by TEM analysis [see Figs. 3(c)–3(e)], which indicates that the antiferroelectric and ferroelectric phases coexist at fields $E < E_{\mathrm{AFE-FE}}$. A schematic representation of the mechanism responsible for temperature evolution of electrocaloric behavior in PNZST is depicted in Fig. 5(b). In the ferroelectric temperature range the electric field always reduces the dipolar entropy by further

aligning the dipoles, leading to a conventional ECE. In the antiferroelectric temperature range the ECE response is determined by the superposition between AFE coupling strength, FE coupling strength, and latent heat contributions. The AFE coupling strength increases with increasing temperature while latent heat decreases when approaching the temperature of the triple point (∼380 K). However, with applied electric field the FE coupling strength intensifies. Hence, the absence of the inverse ECE in the temperature range of antiferroelectric phase up to ∼380 K and at fields $E < E_{\mathrm{AFE-FE}}$ can be rationalized by the coexistence of the antiferroelectric and ferroelectric phases and the released latent heat. The contribution of the latent heat from the field-induced fraction of the FE_R phase (flipping of the polarization) at fields $E < E_{\mathrm{AFE-FE}}$ dominates the ECE and consequently the conventional ECE is observed. With increasing temperature the latent heat reduces and the AFE coupling strength increases, which diminishes the fraction of the field-induced ferroelectric phase. Hence, the ECE gets dominated by the contribution from dipolar entropy of the AFE phase, which causes a crossover from conventional to inverse ECE. The temperature and electric field range of inverse ECE is between 0–3 kV mm^{-1} and 380–410 K. Increasing the applied electric field above 3 kV mm^{-1} provokes again a crossover from inverse to conventional ECE. With increasing electric field, FE coupling strength increases and the ECE is dominated by the contribution from dipolar entropy of the FE phase. Moreover, this concept can be extended to other technologies based on caloric effects, for example ferroics with antiferromagnetic order, which were also reported to exhibit large temperature changes [34].

III. CONCLUSIONS

The isofield and isothermal electric field–temperature phase diagrams were determined for the PNZST antiferroelectric ceramic from dielectric measurements and latent heat studies. The E-T phase diagram reveals the stability of the ferroelectric, antiferroelectric, and paraelectric phases and is augmented by *in situ* TEM to highlight the transient coexistence of AFE and FE phases. The position of the triple point in temperature and electric field space is corroborated by the E-T phase diagrams and the latent heat studies. The temperature- and electric-field-dependent electrocaloric response was correlated with the E-T phase diagram. The decrease of the EC response in the antiferroelectric temperature range and the observed crossover from conventional to inverse ECE was rationalized by considering the impact of the field-induced phase transition and associated latent heat and antiferroelectric coupling strength. We demonstrated the presence of conventional and inverse ECE in antiferroelectric materials, which opens further opportunities to combine both effects and further enhance the cooling efficiency.

[1] B. Atanasiu and P. Bertoldi, Int. J. Green Energy **7**, 552 (2010).

[2] Regulation (EC) No 842/2006 of the European Parliament and of the Council of 17 May 2006 on certain fluorinated greenhouse gases, Official Journal of the European Union L161 (2006) 1–11.

[3] A. S. Mischenko, Q. Zhang, J. F. Scott, R. W. Whatmore, and N. D. Mathur, Science **311**, 1270 (2006).

[4] J. F. Scott, Science **315**, 954 (2007).

[5] M. Valant, Prog. Mater Sci. **57**, 980 (2012).

[6] X. Moya, S. Kar-Narayan, and N. D. Mathur, Nat. Mater. **13**, 439 (2014).

[7] Z. Kutnjak, B. Rožič, R. Pirc, and J. G. Webster, in *Wiley Encyclopedia of Electrical and Electronics Engineering* (John Wiley & Sons, Inc., 2015).

[8] M. E. Lines and A. M. Glass, *Principles and Applications of Ferroelectrics and Related Material* (Oxford University Press, New York, 1977).

[9] F. L. Goupil, A. Berenov, A.-K. Axelsson, M. Valant, and N. M. Alford, J. Appl. Phys. **111**, 124109 (2012).

[10] J. Peräntie, J. Hagberg, A. Uusimäki, and H. Jantunen, Phys. Rev. B **82**, 134119 (2010).

[11] I. Ponomareva and S. Lisenkov, Phys. Rev. Lett. **108**, 167604 (2012).

[12] B. Peng, H. Fan, and Q. Zhang, Adv. Funct. Mater. **23**, 2987 (2013).

[13] R. Pirc, B. Rožič, J. Koruza, B. Malič, and Z. Kutnjak, Europhys. Lett. **107**, 17002 (2014).

[14] W. Geng, Y. Liu, X. Meng, L. Bellaiche, J. F. Scott, B. Dkhil, and A. Jiang, Adv. Mater. **27**, 3165 (2015).

[15] A. A. Heitmann and G. A. Rossetti, J. Am. Ceram. Soc. **97**, 1661 (2014).

[16] R. Pirc, B. Rožič, J. Koruza, G. Cordoyiannis, B. Malič, and Z. Kutnjak, J. Phys.: Condens. Matter **27**, 455902 (2015).

[17] X. Tan, S. E. Young, Y. H. Seo, J. Y. Zhang, W. Hong, and K. G. Webber, Acta Mater. **62**, 114 (2014).

[18] B. Rožič, B. Malič, H. Uršič, J. Holc, B. Kosec, B. Neese, Q. M. Zhang, and Z. Kutnjak, Ferroelectr. **405**, 26 (2010).

[19] D. Berlincourt, H. H. A. Krueger, and B. Jaffe, J. Phys. Chem. Solids **25**, 659 (1964).

[20] D. Viehland, D. Forst, Z. Xu, and J.-F. Li, J. Am. Ceram. Soc. **78**, 2101 (1995).

[21] J. Frederick, X. Tan, and W. Jo, J. Am. Ceram. Soc. **94**, 1149 (2011).

[22] See Supplemental Material at http://link.aps.org/supplemental/10.1103/PhysRevB.97.094113, where the ZFH and ZFC dielectric response is shown, small thermal hysteresis of the antiferroelectric to paraelectric transition is discussed, and the impact of electric field on hysteresis of ferroelectric to antiferroelectric phase transition is demonstrated by showing the temperature evolution of remanent polarization. Supplemental Material includes Refs. [35,36].

[23] Z. Xu, Z. Fan, X. Liu, and X. Tan, Appl. Phys. Lett. **110**, 082901 (2017).

[24] C. Kittel, Phys. Rev. **82**, 729 (1951).

[25] N. Novak, R. Pirc, and Z. Kutnjak, Europhys. Lett. **102**, 17003 (2013).

[26] Z. Kutnjak, R. Blinc, and Y. Ishibashi, Phys. Rev. B **76**, 104102 (2007).

[27] F. Weyland, M. Acosta, J. Koruza, P. Breckner, J. Rödel, and N. Novak, Adv. Funct. Mater. **26**, 7326 (2016).

[28] P. Yang and D. A. Payne, J. Appl. Phys. **71**, 1361 (1992).

[29] N. Novak, R. Pirc, M. Wencka, and Z. Kutnjak, Phys. Rev. Lett. **109**, 037601 (2012).

[30] Z. Kutnjak, J. Petzelt, and R. Blinc, Nature (London) **441**, 956 (2006).

[31] X. Hao, J. Zhai, L. B. Kong, and Z. Xu, Prog. Mater Sci. **63**, 1 (2014).

[32] E. Sawaguchi and T. Kittaka, J. Phys. Soc. Jpn. **7**, 336 (1952).

[33] L. E. Cross, J. Phys. Soc. Jpn. **23**, 77 (1967).

[34] T. Krenke, E. Duman, M. Acet, E. F. Wassermann, X. Moya, L. Manosa, and A. Planes, Nat. Mater. **4**, 450 (2005).

[35] W. Liu and X. Ren, Phys. Rev. Lett. **103**, 257602 (2009).

[36] S. Jesse, B. J. Rodriguez, S. Choudhury, A. P. Baddorf, I. Vrejoiu, D. Hesse, M. Alexe, E. A. Eliseev, A. N. Morozovska, J. Zhang, L.-Q. Chen, and S. V. Kalinin, Nat. Mater. **7**, 209 (2008).